Hydroclimate of the Western United States Based on Observations and Regional Climate Simulation of 1981-2000. Part II: Mesoscale ENSO Anomalies

L. Ruby Leung, Yun Qian, Xindi Bian, and Allen Hunt

Pacific Northwest National Laboratory, Richland, Washington

Abstract

Hydroclimate of the western U.S. is influenced by strong interannual variability of atmospheric circulation, much of which is associated with the El Nino-Southern Oscillation (ENSO). Precipitation anomalies during ENSO often show opposite and spatially coherent dry and wet patterns in the Northwest and California or vice versa. The role of orography in establishing mesoscale ENSO anomalies in the western U.S. is examined based on observed precipitation and temperature data at $1/8^{o}$ spatial resolution and a regional climate simulation at 40 km spatial resolution. Results show that during El Nino or La Nina winters, strong precipitation anomalies are found in northern California, along the southern California coast, and in northwest mountains such as the Olympic Mountain, the Cascades, and the Northern Rockies. These spatial features, which are strongly affected by topography, are surprisingly well reproduced by the regional climate simulation.

A spatial feature we investigated further is the positive-negative-positive precipitation anomaly found during El Nino years in the Olympic Mountain, and on the west side and east side of the Cascades in both observation and regional simulation. Observed streamflows of river basins located in those areas are found to be consistent with the precipitation anomalies. The spatial distribution of the precipitation anomalies is investigated by relating flow direction and moisture to the orientation of mountains and

orographic precipitation. In the west side of the north-south oriented Cascades Range, the increase in atmospheric moisture is not enough to compensate for the loss of orographic precipitation associated with a change in flow direction towards southwesterly during El Nino years. In California, both increase in atmospheric moisture and shift in wind direction towards southwesterly enhances precipitation along the Sierra, which is oriented northwest to southeast. The spatial signature of the interactions between large-scale circulation and topography may provide useful information for seasonal predictions or climate change detection.

1. **Introduction**

Located to the east of the Pacific Ocean, hydroclimate conditions of the western U.S. are strongly affected by large scale atmospheric circulation bringing abundant moisture during the cold season into the continent. Previous studies (e.g., Cayan and Roads 1984; Mitchell and Blier 1997) have established strong correlations between west coast precipitation and mean circulation parameters such as sea-level pressure, 500mb geopotential height, and 850mb moisture advection. Indeed, simple linear models based on observed dependency between precipitation and upper air conditions have been developed to quantify precipitation at a number of locations in California as a function of moisture transport. Such models can explain more than 50% of variance for 5-7 days mean precipitation (e.g., Pandey et al. 1999).

Hydroclimate of the western U.S. is also influenced by strong interannual variability of atmospheric circulation, much of which is associated with the El Nino-Southern Oscillation (ENSO). Studies by Wallace et al (1992), Ropelewski and Halpert (1986), among others provided consistent evidence of coupled atmosphere-ocean variability contributing to climate variability in the North Pacific and western U.S. Composite maps of the warm phase of ENSO (El Nino) show an intensified Aleutian Low and ridging high pressure in the Pacific Northwest (PNW), commonly known as the Pacific North American (PNA) pattern, favoring warm-dry weather in the PNW and cool-wet weather in the Southwest. The opposite is true during the cool phase of the ENSO cycle (La Nina). Therefore, precipitation and temperature anomalies during ENSO often show opposite and spatially coherent warm-dry and cool-wet patterns in the PNW and the Southwest (including southern California and Arizona) or vice versa. They exert major

influence on the interannual variability of surface hydrologic budgets and water resources of the region.

Studies by Redmond and Koch (1991), Dracup and Kahya (1994), Cayan (1996), Dettinger et al. (1998), and Cayan et al (1999) sought to establish the linkage between climate variability and snowpack, streamflow, and hydrologic extremes in the western U.S. They concluded that regional snow anomaly patterns are widespread and associated with anomalous circulation resembling the PNA pattern during ENSO events. Consistent with spatial distribution of ENSO temperature and precipitation anomalies, snowpack anomalies also show out-of-phase pattern in the PNW and Southwest. Furthermore they showed that frequency distribution of daily streamflow from late winter to early summer exhibit strong and systematic response to ENSO variability, and that streamflow response lag the Southern Oscillation Index (SOI), which is used as the ENSO indicator, by a few months. Such a predictive aspect can potentially lead to benefits resulting from the use of seasonal climate forecasts in managing water for flood/drought control and other water uses such as hydropower production and irrigation.

Since the mid-1990s seasonal climate forecasts have been issued by the National Oceanographic and Atmospheric Administration (NOAA) and several other institutions (e.g., Kumar et al. 1996; Livezey et al. 1996; Shukla et al. 2000; Roads et al. 2001) on a routine basis by using statistical and dynamical forecast schemes. The skill of climate forecasts depends strongly from year to year, although in general, it is higher during ENSO events, especially that of the past few strong ENSO cycles (e.g., Kumar and Hoerling 1998), than normal years. To facilitate the use of seasonal climate forecasts for managing resources, modeling systems are being developed to downscale global seasonal

climate forecasts to the regional scales by using statistical methods (e.g., Gershunov 1998), dynamical methods (e.g., Leung et al. 1999; Fennessy and Shukla 2000; Kim et al. 2000), or their combinations (e.g., Gershunov et al. 2000). Studies using regional climate models for downscaling have confirmed the viability of the model nesting approach for generating meaningful, and often improved seasonal anomaly patterns when compared to that of the global models. It is therefore anticipated that climate forecasts at the regional scale may be more useful for water and crop managements, which rely upon spatially explicit climate information.

While the foundation of predictability of large-scale seasonal climate is based mainly upon the interactions of the atmosphere with the slow-varying surface boundary conditions such as sea surface temperature, soil moisture, and snow, predictability of regional scale seasonal climate may also depend upon the interactions between the anomalies of atmospheric circulation and geographic features such terrain, land cover, and oceans or lakes. This may be especially important in the western U.S. where the footprint of interactions between large scale circulation and mesoscale topography shows up clearly in the statistics of seasonal climate discussed in Part I (Leung et al. 2002). The role of orography in establishing mesoscale ENSO anomalies has not been fully explored in previous studies owing to the lack of high spatial resolution observational data and modeling results. This paper will examine the ENSO anomalies in the western U.S. based on observed precipitation and temperature data at $1/8^{o}$ spatial resolution and a regional climate simulation at 40 km spatial resolution. Streamflow data will be examined to check for consistency with the meoscale precipitation and temperature anomalies.

Diagnostics will be performed to elucidate the role of orography in the establishing the ENSO anomaly patterns.

In what follows, we will describe the datasets and regional climate simulation used in this study (Section 2). Section 3 discusses the interannual variability based on observation, the NCEP/NCAR reanalyses, and regional simulation. Section 4 focuses on the ENSO variability and mesoscale features in the climate anomalies. These patterns were further analyzed in two regions over the PNW and California to understand the interactions between large-scale circulation (wind and moisture transport) and orographic forcing along various coastal mountains. Results and conclusions are summarized in Section 5.

2. Datasets and regional climate simulation

Three sets of data have been used to analyze the interannual variability of hydroclimate conditions of the western U.S. The first two datasets are similar to what were used in Part I (Leung et al. 2002). They are the daily maximum and minimum surface temperature and precipitation gridded at $1/8^{o}$ for 1949-2000. This dataset (http://www.hydro.washington.edu/Lettenmaier/gridded_data/) was developed based on station data and covers the conterminous U.S. and the Columbia River basin north of the U.S.-Canada border (Maurer et al. 2001) and has been described by Leung et al. (2002). The second dataset is the NCEP/NCAR reanalyses that were spatial interpolated to the regional climate model domain for our analyses. The third dataset consists of daily streamflow observations made at a number of U.S. Geological Survey gauging stations representing unregulated flows at river basins in the western U.S. The dataset was

compiled by Slack and Landwehr (1992) and extended from 1989-1999 by Iris Stewart and Mike Dettinger (personal communication).

A 20-year regional climate simulation performed using the Penn State/NCAR Mesoscale Model MM5 (Grell et al. 1993) driven by the NCEP/NCAR reanalyses has been described in detail in Part I (Leung et al. 2002), which describes evaluation of the simulated seasonal statistics. The simulation was initialized on July 1980 with lower and lateral boundary conditions updated every 6 hours based on the NCEP/NCAR reanalyses large-scale conditions. Simulation was performed using a nested configuration with the larger domain covering the whole U.S. and surrounding oceans at 120 km resolution and the nested domain covering the western U.S. at 40 km resolution. Analyses were performed using simulation at the nested domain from 1 September 1980 to 30 June 2000. In this paper, we focus on investigating the interannual variability simulated by the model and compare that with observations. In particular our emphasis is on climate variability associated with the ENSO events.

3. Interannual variability

Figures 1 and 2 depict the interannual variability of temperature and precipitation for the warm and cold seasons. The regional simulation generally exhibits realistic variability in surface temperature across the region. During the cold season, variability is strongest in the northeast part of the domain, reaching 2-3°C, and smallest along the coast and southwestern U.S. Variability during the warm season is smaller and fairly uniformly distributed between 1–1.5^{o}C across the region. The temperature variability is generally larger than the observed in the Northwest in both the reanalyses and regional simulation

during summer. During winter, the regional simulation shows stronger variability comparable to the observed in the Northern Rockies than the reanalyses.

An interesting feature to note is the appearance of localized regions of strong temperature variability (up to 4.5^{o}C) over the central Rockies during winter, and that over the southwest during summer in the observations. The latter, probably related to variability of the North American Monsoon, is less coherent spatially and does not appear to be correlated with topography everywhere. These smaller areas of strong temperature variability are neither found in the regional simulation nor the reanalyses. Possible reasons are insufficient snow simulated in the Rockies during winter and rain in the Southwest during summer that led to reduced snow-albedo and land-atmosphere feedbacks, which result in smaller interannual variability.

There is more spatial structure associated with the normalized interannual variability in precipitation as shown in Figure 2. Areas with values below zero are used to locate regions with mean seasonal mean precipitation less than 1 mm/day. During winter, the largest normalized variability is found in California, especially over the Sierra and southern California, and the Southwest where the variance is equal to 50-80% of the seasonal mean. These are also areas where larger extreme precipitation is found (Leung et al. 2002). Variability in the Northwest is generally only 20-30% of the seasonal mean. The regional simulation captures the spatial distribution and magnitude of the normalized precipitation variability much better than the reanalyses during winter.

During summer, the normalized variability is typically larger along coastal mountains and the Rockies, reaching up to 30% of the seasonal mean. The regional simulation shows similar spatial pattern of variability, the strongest of which is along coastal

mountains during summer. However, there is less variability simulated over the Rockies and the Southwest than observed. Variability in the Northwest is over-simulated by the reanalyses. The influence of topography is evident in both seasons. At much coarser spatial resolution, the variability in the reanalyses has broader spatial features and is generally less than that of the observations or regional simulation, except near the Great Basin during summer.

The large interannual climate variability in the Northwest and California is further illustrated in Figure 3, which shows the observed and simulated temperature and precipitation anomalies averaged over the two regions. The timing and magnitude of regional anomalies are realistically simulated by the regional climate model at 40 km resolution. Similar to previous findings using mesoscale models such as MM5 in regional climate modeling (e.g., Leung and Ghan 1998; 1999), the simulated temperature and precipitation in the long-term integrations remain consistent with the observed and that of the global reanalyses used to provide boundary conditions for the simulations. There is no sign of model drift or instability in the 20-year simulation. Figure 3 shows that temperature and precipitation quite often vary in an opposite direction. That is, anomalies tend to occur in dry-warm or wet-cool patterns simultaneously (e.g., 1992-1995). In Section 4, we will focus on climate variability associated specifically with the ENSO events, which represent the dominant mode of variability in the western U.S.

4. ENSO Variability

a. Temperature, precipitation, and streamflow anomalies

It is generally accepted that temperature and precipitation tends to vary as a whole within regions such as the Northwest and California, and therefore spatial variations are

less important when looking at interannual variability than seasonal means, which have spatial distribution highly resembling that of the terrain. We will examine the ENSO anomalies using observational and simulation data at spatial resolution higher than that typically used in the past to determine if mesoscale patterns exist within the larger scale coherent spatial structures. Using the Southern Oscillation Index (SOI), defined as the standardized difference in sea level pressure anomalies between Tahiti and Darwin, to classify El Nino years when SOI is -0.5 or less and La Nina years when SOI is 0.5 or greater, we selected 1983, 1987, 1988, 1992, 1995, and 1998 as El Nino years and 1984, 1985, 1986, 1989, and 1999 as La Nina years for our analyses. With observation and simulation at 40 km resolution or higher, we examined the spatial distribution of ENSO anomalies and investigated how mesoscale topography may play a role in determining the spatial features.

Figure 4 shows the observed, reanalyzed, and simulated composite El Nino anomalies of precipitation and temperature during 1980-2000. Anomalies are estimated based on the difference between mean El Nino year conditions and long term mean conditions. At the larger scale, the major patterns of precipitation variations are the dry anomalies in the Rockies and wet anomalies along the Pacific coast, especially in northern California. Temperature is generally cooler than normal in the south and warmer than normal by up to 2°C towards the north. Areas with the largest wet anomalies are associated with small or near zero temperature anomalies in northern California. Areas with dry anomalies in the Rockies are associated with larger warm anomalies. These patterns are consistent with results of earlier studies and the anomalies shown in Figure 3.

Although much of the climate variations in the western U.S. are captured at the larger scales, the effects of topography are not negligible. Most notably, the largest dry anomalies during El Nino years in the Northwest are found on the windward side of the Cascades and the Northern Rockies. The rest of the Northwest region typically shows very small anomalies except on the lee side of the mountains (e.g., northeast of the Olympic Mountain and the Cascades) where regions of positive anomalies are often found instead. The largest wet anomalies are located in northern California and along the Sierra and the southern coast.

The NCEP/NCAR reanalyses only captures the very broad spatial features of the temperature and precipitation anomalies, namely the gradual increasing warming trend towards the north, and the wet and dry anomalies along the coast and further inland. The regional simulation represents a clear improvement over the NCEP/NCAR reanalyses that provided the large-scale conditions for driving the simulation. It correctly captures the larger scale feature, namely the near north-south gradient in temperature and precipitation anomalies, as well as some of the mesoscale features associated with the complex terrain such as the positive-negative-positive anomalies on northeast Olympic Mountain and windward and lee side of the Cascades, and the large wet anomalies in northern California. The simulated precipitation anomalies in the southern Sierras are, however, too strong compared to observations. The temperature anomalies in the regional simulation are more realistic than the reanalyses, with stronger warming over Canada and stronger cooling in the Southwest.

During La Nina years, Figure 5 shows cooler temperature over much of the Northwest and northern California with anomalies reaching –3°C in the Snake River

Valley. Warmer anomalies typically less than 1°C are found over the Southwest. Combining Figures 4 and 5, our analyses show that the Northwest is marked by warm-dry conditions during El Nino years and cool-wet conditions during La Nina years. In the Southwest (southern California and Arizona), climate varies between cool-wet and warm-dry instead during El Nino and La Nina years respectively. In northern California, precipitation anomalies are large, but temperature variability is very small.

Comparing the NCEP/NCAR reanalyses and the regional simulation, the latter correctly shows more extensive warm anomaly in the Southwest, and stronger cold anomaly in southern Idaho. For precipitation, the Northwest is dominated by wet anomalies of up to 1 mm/day in coastal mountains and the Rockies; larger wet anomalies are found along the windward side of the Olympic Mountain and the Cascades. Large dry anomalies are found in much of California, the strongest of which are located along coastal mountains, the Sierra, and southern coastline. While the NCEP/NCAR reanalyses generally agree with observations at the large scale, the regional simulation displays spatial characteristics very similar to the observed. Generally for both El Nino and La Nina conditions, anomalies are amplified on the windward side of the Cascades and the Sierra, and sometime anomalies of opposite signs can be found on the lee side. These features are robust in the observations, as we have analyzed the full 50 years period based on the 1/8° data and found similar spatial characteristics. Furthermore models can reproduce those features, provided that sufficient spatial resolutions are used to represent mountain effects.

How significant are the ENSO temperature and precipitation anomalies? We calculated the signal-to-noise ratio based on the mean anomalies and interannual

variability for El Nino and La Nina years. During El Nino years, the magnitude of the signal-to-noise ratio in observed temperature anomaly reaches 0.6 – 1.0 in the Southwest and PNW in Washington and Oregon. For precipitation, the ratio is 0.6-1.0 in the western half of California, southern California and Nevada, and northern Rockies. During La Nina years, ratios of similar magnitude are found in isolated regions of the Southwest and eastern Oregon and Idaho for temperature anomaly. For precipitation anomaly, such high signal-to-noise ratios are found over the majority of the Southwest, east of the Sierra, and Northern Rockies. The signal-to-noise ratios in the regional simulation are comparable to that of the observations. They are generally larger than that based on the reanalyses especially for precipitation anomalies.

Before we investigate the mesocale features of ENSO precipitation anomalies further, we check for consistency with streamflow anomalies. Figure 6 shows the El Nino year and long-term mean streamflows at the Columbia River and Sacramento-San Joaquin Basin during the last 50 years. El Nino anomalies of streamflow in the Columbia River are dominated by the more extensive dry anomalies in the mountains of the Northwest; reduced precipitation and warmer temperature imply less snow and a lower peak runoff. In the Sacramento-San Joaquin Basin, more precipitation and slightly warmer temperature during El Nino years contribute to increased runoff from winter through early summer.

Although streamflows in large river basins reflect the large-scale temperature and precipitation anomalies in the Northwest and California, streamflows at smaller river basins can display streamflow anomalies that reflect the effects of local temperature and precipitation anomalies. Figure 7 show the streamflows at 6 river basins in the Northwest

averaged over El Nino years and the whole 20 years period. These river basins are located in areas where positive-negative-positive anomalies as discussed above are found near the Olympic Mountain and the Cascades. Furthermore they represent features of transition from coastal watersheds to inland snow-dominant watersheds. The Duckabush River and North Fork Skokomish lie on the northeast of the Olympic Mountain. These are mainly rain-fed basins with runoff more directly related to the timing of precipitation. During El Nino years, positive precipitation anomalies (as shown in Figure 4) in these areas show up distinctly as increases in runoff during the cold season (January-March). Annual total runoff increases by 4% and 2.5% respectively during El Nino years as compared to long-term averages. Runoff during the cold season has larger increases of 15-20% during El Nino years.

The Skykomish and Snoqualmie River are located on the west of the Cascades where El Nino precipitation anomalies are more strongly negative. These are typical mixed rain and snow basins with double runoff peaks in early winter and summer. During El Nino years, reduced precipitation during the cold season is reflected in large reduction in runoff between November and February. Reduced snowmelt and warmer temperature also affect the magnitude and timing of the second peak in the hydrographs, which is fed mainly by snowmelt. Impacts on streamflow therefore extend beyond the cold season. Annually, total streamflow is reduced by 14% in both basins.

Lying on the east of the Cascades, the Andrews and the Methow River are snowmelt-dominated basins with a single runoff peak during early summer that corresponds to peak snowmelt. During El Nino years, precipitation anomalies are slightly positive. However, streamflow in this type of basins is governed by the combined effects of temperature and

precipitation. With the cold temperature, increased precipitation in the cold season during El Nino years is not reflected directly in increased runoff because a large percentage of precipitation falls in the form of snow and accumulates on the ground rather than enters the stream. The effect of warmer temperature during El Nino years, however, appears in earlier snowmelt and hence a shift in the runoff peak by about a month earlier. The annual total streamflows during El Nino years are 2.4% and 0.5% less than the long-term average respectively in the two river basins; they do not reflect changes in precipitation during the cold season. The above analyses show that the observed streamflow anomalies are generally consistent with El Nino temperature and precipitation anomalies near the Olympic Mountain and the west and east sides of the Cascades.

b. Large scale circulation and topographic control on ENSO anomalies

1) PACIFIC NORTHWEST

To understand the impacts of orography on the mesoscale ENSO anomalies, we first analyzed the relationships between circulation and precipitation during the cold season. Our analysis is based on the regional simulation alone because it was able to reproduce the mesoscale features being studied. In addition, the simulated large-scale circulations such as 850 mb wind and moisture near the Pacific coast are in close agreement with the NCEP/NCAR reanalyses, which included assimilation of the vertical profiles of observed wind and humidity. We first restrict our analysis to the Pacific Northwest since more interesting signals of positive and negative signs are found in the mesocale anomalies. Three regions corresponding to locations with positive-negative-positive precipitation anomalies near the Olympic Mountain and the west and east sides of the Cascades are

selected. The anomaly correlations between monthly mean zonal wind and the zonal component of moisture flux along the Pacific coast (near 125°W and 45°N) with precipitation are 0.89 and 0.86 respectively showing significant impacts of zonal flow and moisture flux on precipitation events in the Northwest. Figure 8 shows the locations selected for the analyses of daily wind, moisture flux, and precipitation during winter.

Figure 9 shows the total moisture flux as a function of wind direction and frequency distribution of wind direction for various precipitation thresholds at the three regions. Larger total moisture flux is associated with southwesterly flows from the warmer Pacific Ocean. For light precipitation events between 0 and 1 mm/day, there is a near uniform or slightly bimodal distribution of wind direction clustered near northerly and southerly flows. During days with moderate precipitation between 1 and 10 mm/day, the distribution of wind direction follows closely the distribution of the total moisture flux. For more intense precipitation between 10 and 30 mm/day, the distribution of wind direction becomes much narrower and concentrated near the southwesterly flows. The distribution on the west of the Cascades is different from that of the other two regions; the secondary peak near westerly flows indicates that flows perpendicular to the Cascades Range and orographic effects are important for generating intense precipitation on the windward side of the mountain.

A plot (not shown) of the distributions of total moisture flux as a function of wind direction during El Nino winters and normal winters show similar distributions which maximized in the southwesterly direction. There is, however, an increase of total moisture flux by about 23% during El Nino years compared to normal years, and the increase is main associated with southwesterly flows. This increase in moisture flux is

consistent with the change in the frequency distribution of wind direction as shown in Figure 10. During El Nino years, the frequency distribution is narrower and the mean wind direction shifts from about 265° near westerly during normal years to about 248° towards more southwesterly. These changes in total moisture flux and wind direction will have important impacts on precipitation. Figure 11 shows the precipitation distribution as a function wind direction averaged over El Nino and Normal years. Under normal conditions, precipitation in the Olympic Mountain and east of the Cascades both exhibit strongest precpitation for southwesterly flows. However on the west of the Cascades, westerly flows are equally important for generating precipitation because, as discussed above, orographic forcing is strongest for flows that are perpendicular to the north-south oriented mountain range.

During El Nino years, there is a decrease in precipitation at all three regions associated with flows near 250° that is mainly related to the reduced frequency of such events as evidenced in Figure 10. The reduction in precipitation caused by such a change in flow frequency is largest on the west of the Cascades because orographic precipitation is much reduced. At the Olympic Mountain (which is circular and therefore has no preferred direction of orographic forcing) and east of the Cascades, the increase in precipitation related to the increased moisture flux and frequency of flows near 225° more than compensate for the loss of precipitation associated with the reduced frequency of flows near 250° to create positive precipitation anomaly during El Nino years. On the west of the Cascades, the increase in moisture flux and frequency of flows near 225° has very little impact on precipitation because orographic forcing is weak for southwesterly flows impinging on a north-south oriented mountain range. The increase in moisture has

a stronger impact for flows near 270° on the windward facing slope. However, because of reduced frequency of flows near 250°, the effect of increased moisture flux near 270° is not strong enough to compensate for the loss of precipitation associated with reduced frequency of flows near 250°. As a result, El Nino precipitation anomaly is negative on the west side of the Cascades.

As a further illustration of how wind direction affects orographic precipitation in the Northwest mountains, Figure 12 shows the precipitation associated with flows near 270° and 250°, which correspond to mean flow directions during Normal and El Nino years, along a east-west transect along 47.8^{o}N. The transect is 40 km wide and cuts across the Olympic Mountain, the Cascades, upper Columbia Basin, and the Northern Rockies. Note that more moisture is typically associated with flows near 250° coming from the warmer side of the Pacific Ocean than westerly flows. For westerly flow, orographic precipitation is particularly strong on the west of the Cascades. As a result of changes in flow direction and moisture content, the difference between the precipitation associated with the two flow regimes exhibit a positive-negative-positive pattern that is similar to the El Nino anomalies. The change in sign between the difference in precipitation associated with the two flow regimes from the Olympic Mountain to the west and east of the Cascades is clear and physically consistent with the interactions of wind with the underlying topography. Therefore the spatial distribution of the El Nino precipitation anomaly near the coast, along the Cascades, in the Columbia Basin, and the Northern Rockies can be generally explained by the interactions between changes in wind direction and moisture flux with the underlying topographic features of the Northwest.

2) NORTHERN CALIFORNIA

The large positive El Nino precipitation anomaly in California can be more easily explained by changes in large-scale circulation. We analyzed the wind and moisture flux off shore northern California, near 123°W and 38°N, and precipitation at two locations on the southern Cascades and Sierra indicated in Figure 7. Figure 13 shows the frequency distributions of precipitation as a function of wind direction for different precipitation thresholds and the distribution of moisture flux. Light precipitation events (between 0 and 1 mm/day) are more related to northerly and northwesterly flows. There is a more gradual transition in the frequency distribution from light to heavy precipitation events in northern California than the Northwest. For heavy precipitation, the frequency distribution at the Cascades peak near 250°. In the southern Sierra, there is a secondary peak at 225° that corresponds to flows perpendicular to the Sierra Range. Again, this is a manifestation of stronger orographic uplifts for flows perpendicular to the mountain ridge.

Figure 14 shows the distribution of wind direction during El Nino and Normal years. The shift in wind direction during El Nino years near California is even more profound than that in the Northwest. During El Nino years, there are clearly reduced frequency of northerly to northwesterly flows and increased frequency of westerly to southwesterly flows with 22% increase in total moisture flux associated predominantly with southwesterly flows. In the Sierra, changes in moisture flux and wind direction both favor stronger precipitation for the terrain features. As a result, El Nino precipitation anomaly is positive and reflects the effects of circulation changes and orographic enhancement. This is shown in Figure 15 that shows the frequency distribution of precipitation as a

function of wind direction during El Nino and Normal years. Over the Cascades, changes in moisture flux and increase in flow frequency for all flows between 200° and 270° are responsible for the increased precipitation. On the Sierra, particularly the southern area, more increase in precipitation is associated with wind directions between 200° and 225° which are the preferred flow direction for orographic forcing in the northwest-southeast oriented mountain range. We note, however, that the simulated precipitation anomaly in southern Sierra is too high compared to observation (see Figure 4). Because the regional climate model simulates too much orographic precipitation in the Sierra (see results of Part I), it also exhibits higher sensitivity to changes in circulation and its interactions with the underlying topography than observed.

Summarizing the analyses for the whole western U.S., unless a model correctly captures both changes in large-scale circulation during ENSO events and orographic effects of mountains on precipitation, mesoscale ENSO precipitation anomaly features cannot be precisely predicted. This will have important implications to seasonal climate predictions and their applications to water resources in regions of complex terrain.

5. Conclusions

Detailed analyses and evaluation have been reported in this study to investigate how well regional climate simulations capture interannual variability, especially that associated with ENSO, in the western U.S. Results show strong interannual variability in temperature, up to 5°C, exist in the Rockies during winter, and smaller variability up to 2°C is found during summer. Precipitation variability is particular high in California and the Southwest during winter. Compared to the reanalyses, the regional climate simulation

provides more realistic description of the magnitude and spatial distribution of interannual variability.

In the western U.S., precipitation anomaly associated with the ENSO events exhibits strong spatial variations that were not captured by the NCEP/NCAR reanalyses. During El Nino or La Nina winters, strong anomalies are found in northern California, along the southern California coast, and in northwest mountains such as the Olympic Mountain, the Cascades, and the Northern Rockies. These spatial features are surprisingly well reproduced by the regional climate simulation. Spatial distributions of precipitation anomaly are found to be strongly affected by terrain features of the region. We found positive-negative-positive precipitation anomaly during El Nino years in the Olympic Mountain, and on the west side and east side of the Cascades in both observation and regional simulation. Observed streamflows of river basins located in those areas are found to be consistent with the precipitation anomalies. This indicates that noticeable effects on streamflows at the regional scales can be of opposite sign to that of the larger river basins, which is mainly negative during El Nino years for major tributaries of the Columbia River. Continuous progress in predicting ENSO temperature and precipitation anomalies will potentially lead to useful climate forecasts for managing water resources in the western U.S.

To understand how topography interacts with large-scale circulation to produce the mesoscale features, we analyzed 850mb wind and moisture transport near the Washington and California coasts and precipitation in the Olympic Mountain, the Cascades, and the Sierra Range. During El Nino years, there is a shift in wind direction from westerly towards southwesterly, which is accompanied by an increase of

atmospheric moisture. For the north-south oriented Cascades, the increase in moisture is not enough to compensate for the loss of precipitation due to reduced orographic forcing on the west side of the Cascades with the more southwesterly flows. Quite the opposite, the Olympic Mountain and the east of the Cascades receive more precipitation during El Nino years due to increase in atmospheric moistures. The east of the Cascades also benefits from reduced orographic blocking associated with the more southwesterly flows. In California, both increase in atmospheric moisture and shift in wind direction towards southwesterly enhances precipitation along the Sierra, which is oriented northwest to southeast. Much of northern California receives more precipitation during El Nino years than Normal years.

This study suggests that when realistic large-scale circulations are used to drive regional climate models, ENSO anomalies can be correctly simulated at the regional scales. The important improvements in the regional simulation over the reanalyses (which provides boundary conditions for the regional model) may be partly related to different physics parameterizations used in the global model producing the NCEP/NCAR reanalyses and the regional model. Higher spatial resolution in the regional model also results in improved dynamics and more detailed representation of topography and land cover, which provide important regional forcings for more realistic simulations of climate sensitivity. Similar improvements may be expected when the regional models are driven by GCMs rather than reanalyses, as have been demonstrated preliminarily by Leung et al. (1999) and Fennessy and Shukla (2000).

On the predictability of seasonal climate anomalies at the regional scale, one important question is whether the signal-to-noise ratio at the regional scale is smaller

than, comparable to, or larger than that at the larger or continental scale. Results from Fennessy and Shukla (2000) suggested that the signal-to-noise ratio based on the nested modeling results is larger than that of the global forecasts. If this were true, climate forecasts with the nested modeling approach may require less than or at most comparable ensemble size to that used in the global modeling system. This may be possible if ENSO anomalies at the regional scales are much amplified to overcome the increase in interannual variability at the same scales. This is indeed found to be true in some regions of the western U.S. such as the Southwest and northern California where signal-to-noise ratio is enhanced at the regional scales in the observation and regional simulation compared to the coarse scale reanalyses.

Interactions between large-scale circulation and topography not only amplify ENSO anomalies of temperature and precipitation at the regional scales, streamflow and snowpack anomalies are even more accentuated because temperature and precipitation in both the wet-dry and cool-wet patterns reinforce one another to accentuate changes in snowpack and streamflow. This has important implications for both seasonal prediction and climate change sensitivity: topography may act to amplify regional climate signal (e.g., Giorgi et al. 1997; Leung and Ghan 1999), and even more so in hydrologic signal (Leung and Ghan 1999; Cayan et al. 1999), to an extent that amplification in mesoscale noise is overcome. Contrary to the general belief that predictability decreases as spatial scale decreases which is true for chaotic systems, the deterministic nature of interactions between large-scale circulation and topography may potentially extend predictability of the climate system. The footprint or spatial signature of the interactions may provide useful information for seasonal predictions or climate change detection. This issue

requires and deserves much further investigation with a combination of high spatial resolution observational data and simulation results.

Acknowledgment. Funding for this study was provided by the Department of Energy Accelerated Climate Prediction Initiative (ACPI), the Joint Institute for the Study of Atmosphere and Oceans (JISAO) Climate Impacts Group (CIG) at the University of Washington, and the National Oceanic and Atmospheric Administration (NOAA) Global Energy and Water Cycle Experiment (GEWEX) Americas Prediction Project (GAPP). The ACPI Pilot effort was supported largely by the DOE Office of Biological and Environmental Research through numerous contracts and subcontracts to the participants. The CIG is supported by the NOAA Office of Global Programs. All regional climate simulations reported in this study were performed on 64 processors of an IBM-SP3 at the Center for Computational Sciences (CCS), which is supported by the DOE Office of Science, at the Oak Ridge National Laboratory (ORNL). The authors thank Iris Stewart and Mike Dettinger of U.S. Geological Survey and Scripps Institution of Oceanography (SIO) for providing the observed streamflow datasets. Pacific Northwest National Laboratory is operated for the U.S. Department of Energy by Battelle Memorial Institute under Contract DE-AC06-76RLO 1830.

Corresponding author address: Dr. L. Ruby Leung, Pacific Northwest National Laboratory, P.O. Box 999, Richland, WA 99352. E-mail: ruby.leung@pnl.gov

REFERENCES

Cayan, D.R., 1996: Interannual climate variability and snowpack in the western United States. *J. Clim*., **9**, 928-948.

-----, and J.O. Roads, 1984: Local relationships between United States west coast precipitation and monthly mean circulation parameters. *Mon. Wea. Rev*., **112**, 1276-1282.

-----, K.T. Redmond, and L.G. Riddle, 1999: ENSO and hydrologic extremes in the western United States. *J. Clim*., **12**, 2881-2893.

Dettinger, M.D., D.R. Cayan, H.F. Diaz, and D.M. Meko, 1998: North-south precipitation patterns in western North America on interannual-to-decadal timescales. *J. Climate*, **11**, 3095-3111.

Dracup, J.A., and E. Kahya, 1994: The relationships between U.S. streamflow and La Nina events. *Water Resour. Res*., **30**, 2133-2141.

Fennessy, M.J., and J. Shukla, 2000: Seasonal prediction over North America with a regional model nested in a global model. *J. Clim*., **13**, 2605-2627.

Gershunov,A., 1998: ENSO influence on intraseasonal extreme rainfall and temperature frequencies in the contiguous United States: Implications for long-range predictability. *J. Clim*., **11**, 3192-3203.

Gershunov, A., T. P. Barnett, D.R. Cayan, T. Tubbs, and L. Goddard, 2000: Predicting and downscaling ENSO impacts on intraseasonal precipitation statistics in California: The 1997/98 event. *J. Hydrometeorol*., **1**, 201-210.

Giorgi, F., J.W. Hurrell, M.R. Marinucci, and M. Beniston, 1997: Elevation dependency of the surface climate signal: A model study. *J. Clim*., **10**, 288-296.

Grell, G., J. Dudhia, and D.R. Stauffer, 1993: A description of the fifth generation Penn State/NCAR mesoscale model (MM5). *NCAR Tech. Note., NCAR/TN-398+IA*, Nat. Cent. for Atmos. Res., Boulder, CO.

Kim, J., N.L. Miller, J.D. Farrara, and S.-Y. Hong, 2000: A seasonal precipitation and stream flow hindcast and prediction study in the western United States during the 1997-98 winter season using a dynamic downscaling system. *J. Hydrometeorol*., **1**, 311-329.

Kumar, A. and M. Hoerling, 1998: Annual cycle of Pacific-North American seasonal predictability associated with different phases of ENSO. *J. Clim*., **11**, 3295-3308.

-----, -----, M.Ji, A. Leetmaa, and P. Sardeshmukh, 1996: Assessing a GCM's suitability for making seasonal predictions. *J. Clim*., **9**, 115-129.

Leung, L.R., and S.J. Ghan, 1999: Pacific Northwest climate sensitivity simulated by a regional climate model driven by a GCM. Part II: 2xCO2 simulations. *J. Clim*., **12**, 2031-2053.

-----, A.F. Hamlet, D.P. Lettenmaier, and A. Kumar, 1999: Simulations of the ENSO hydroclimate signals over the Pacific Northwest Columbia River Basin. *Bull. Amer. Meteorol. Soc*., **80(11)**, 2313-2329.

-----, Y. Qian, and X. Bian, 2002: Hydroclimate of the western United States based on observation and regional climate simulation of 1981-2000. Part I: Seasonal statistics. *J. Clim*., submitted.

Livezey, R.E., M. Masutani, M. Ji, 1996: SST-forced seasonal simulation and prediction skill for versions of the NCEP/MRF model. *Bull. Amer. Meteorol. Soc*., **77**, 507-517.

Maurer, E.P., G.M. O'Donnell, D.P. Lettenmaier, and J.O. Roads, 2001: Evaluation of the land surface water budget in NCEP/NCAR and NCEP/DOE Reanalyses using an off-line hydrologic model. *J. Geophys. Res*., **106(D16)**, 17,841-17,862.

Mitchell, T.P., and W. Blier, 1997: The variability of wintertime precipitation in the region of California. *J. Clim*., **10**, 2261-2276.

Pandey, G.R., D.R. Cayan, and K.P. Georgakakos, 1999: Precipitation structure in the Sierra Nevada of California during winter. *J. Geophy. Res*., **104**, 12019-12030.

Redmond, K.T., and R.W. Koch, 1991: Surface climate and streamflow variability in the western United States and their relationship to large scale circulation indices. *Water Resour. Res*., **27**, 2381-2399.

Roads, J.O., S.-C. Chen, and F. Fujioka, 2001: EPCP's weekly to seasonal global forecasts. *Bull. Amer. Meteorol. Soc*., **82**, 639-658.

Ropelewski, C.F., and M.S. Halpert, 1986: North American precipitation and temperature patterns associated with the ENSO. *Mon. Wea. Rev*., **114**, 2352-2362.

Shukla, J., and Coauthors, 2000: Dynamical seasonal prediction. *Bull. Amer. Meteor. Soc*., **81**, 2598-2606.

Slack, J.R., and J.M. Landwehr, 1992: Hydro-Climatic Data Network (HCDN): A U.S. Geological Survey streamflow data set for the United States for the study of climate variations, 1874-1988. *U.S. Geological Survey Open-File Rep. 92-129*, 200pp. [Available from U.S. Geological Survey, Books and Open File Reports Section, Federal Ctr., Box 25286, Denver, CO 80225.]

Wallace, J.M., C. Smith, and C.S. Bretherton, 1992: Singular value decomposition of wintertime sea surface temperature and 500-mb height anomalies. *J. Clim.*, **5**, 561-576.

FIGURE CAPTIONS

Figure 1. Standard deviation of seasonal mean surface temperature based on NCEP/NCAR reanalyses (top), simulation (middle), and observation (bottom) for warm (left) and cold (right) seasons. Contour intervals are 0.4 ^{o}C.

Figure 2. Similar to Figure 1, but for normalized standard deviation of seasonal mean precipitation. Contour intervals are 0.2. Area with precipitation less than 1 mm/day are shaded in purple with values less than 0.

Figure 3. Mean annual surface temperature and precipitation anomalies averaged over the Pacific Northwest and California based on simulation (right) and observation (left). Units are ^{o}C for temperature and mm/day for precipitation.

Figure 4. Anomalies of surface temperature (^{o}C) (right) and precipitation (left) during El Nino years between 1981-2000 based on NCEP/NCAR reanalyses (top), regional simulation (middle) and observation (bottom) for January-February-March.

Figure 5. Similar to Figure 4, but for anomalies during La Nina years.

Figure 6. Observed streamflow averaged over El Nino years and all years during the last 50 years at the Columbia River and Sacramento-San Joaquin River basins. Unit is m^3/s.

Figure 7. Observed streamflow averaged over El Nino years and all years between 1981-2000 at the Duckabush River and North Fork Skokomish near the Olympic Mountain, Skykomish River and Snoqualmie River on the west of the Cascades, and Andrews and Methow River on the east of the Cascades. Unit is m^3/s.

Figure 8. Nested domain of the regional simulation showing locations of wind analyses (open circles) and precipitation (squares) in the Northwest and California.

Figure 9. Frequency distribution of wind direction for different precipitation thresholds (thin lines) between 0 to 30 mm/day, and distribution of total moisture flux (g/kg m/s) as a function of wind direction (thick line) at (a) Olympic Mountain, (b) west of the Cascades, and (c) east of the Cascades based on regional simulation. Note that wind direction is defined as 0 for northerly, 90 for easterly, and 180 for southerly respectively.

Figure 10. Frequency distribution of wind direction at the Pacific coast near Northwest averaged over Normal and Warm ENSO (or El Nino) years during 1981-2000 based on regional simulation.

Figure 11. Similar to Figure 10, except for distribution of precipitation (mm/day) as a function of wind direction for the three Pacific Northwest regions shown.

Figure 12. Precipitation (mm/day) at an east-west transect across the Pacific Northwest averaged over January-February-March for near westerly flows (W) between 270-280° and towards southwesterly flows (SW) between 250-260° based on regional simulation. Also shown are the difference in precipitation associated with the two flow regimes and surface elevation (100m) of the transect.

Figure 13. Similar to Figure 9, but for analyses in California at (a) southern Cascades, (b) northern Sierra, and (c) southern Sierra.

Figure 14. Similar to Figure 10, but for wind off the coast of California.

Figure 15. Similar to Figure 11, but for precipitation over three regions in California.

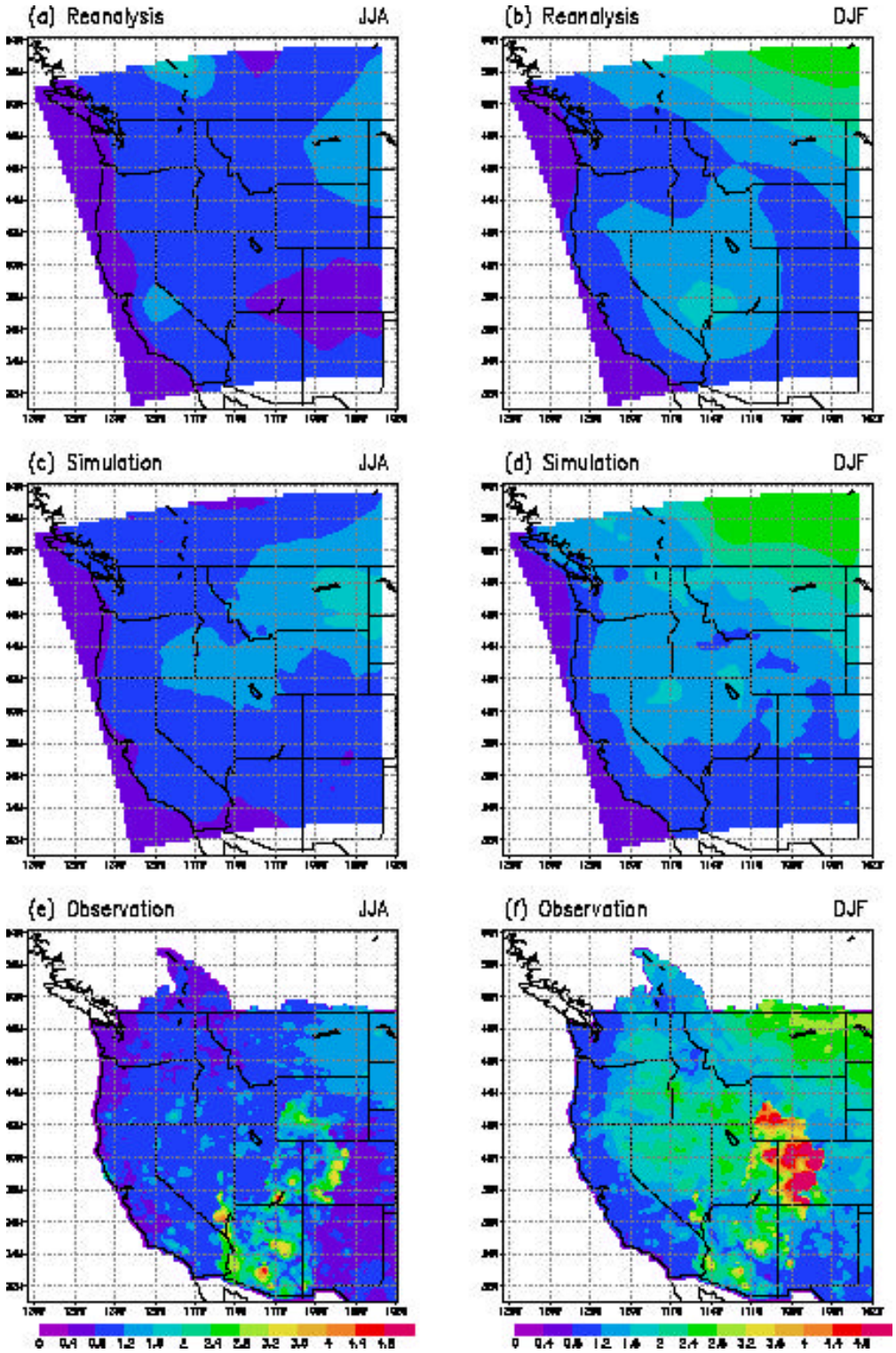
(a) Reanalysis
JJA
(b) Reanalysis
DJF
(c) Simulation
JJA
(d) Simulation
DJF
(e) Observation
JJA
(f) Observation
DJF

Figure 1

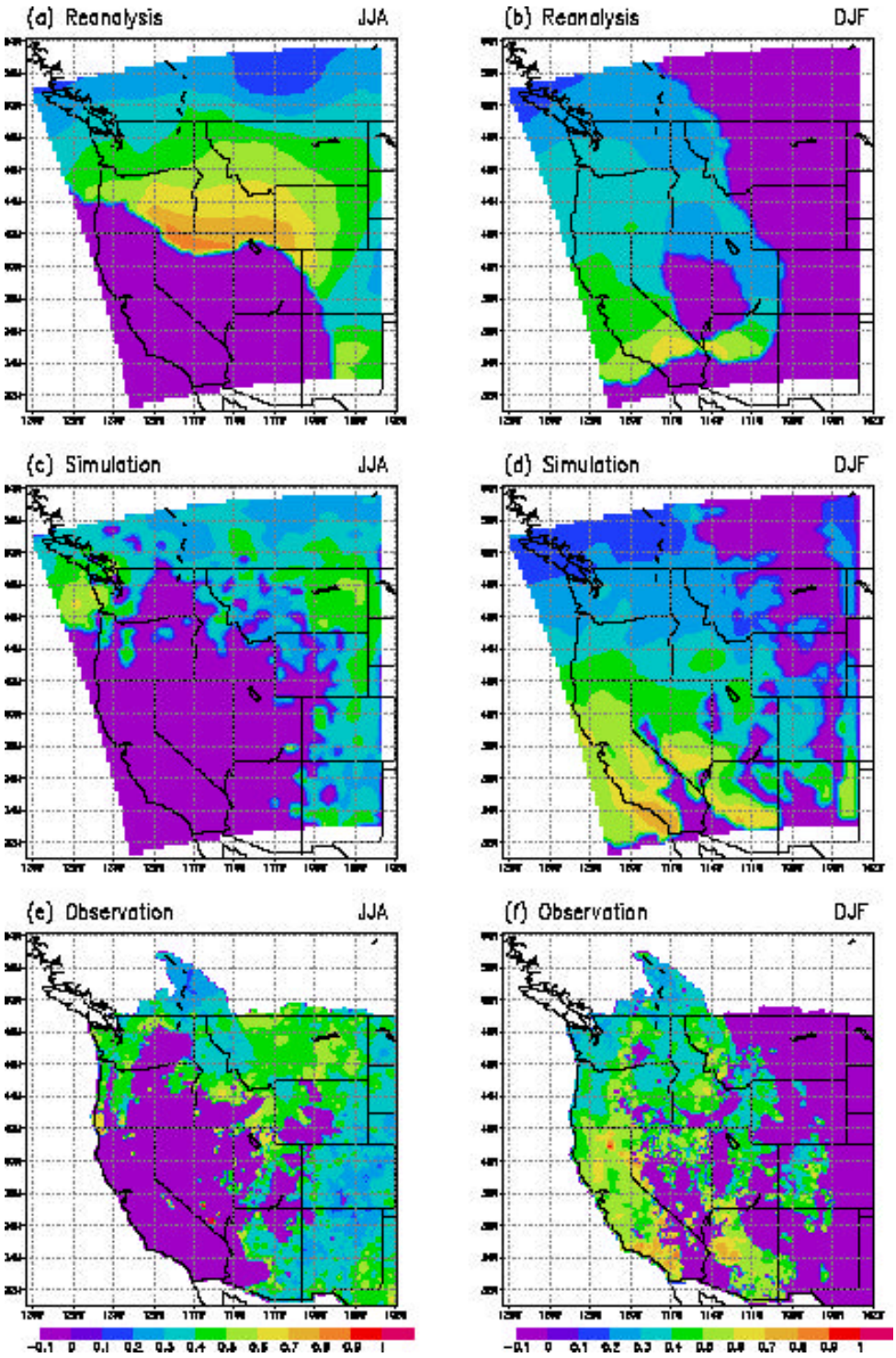
(a) Reanalysis JJA
(b) Reanalysis DJF
(c) Simulation JJA
(d) Simulation DJF
(e) Observation JJA
(f) Observation DJF

Figure 2

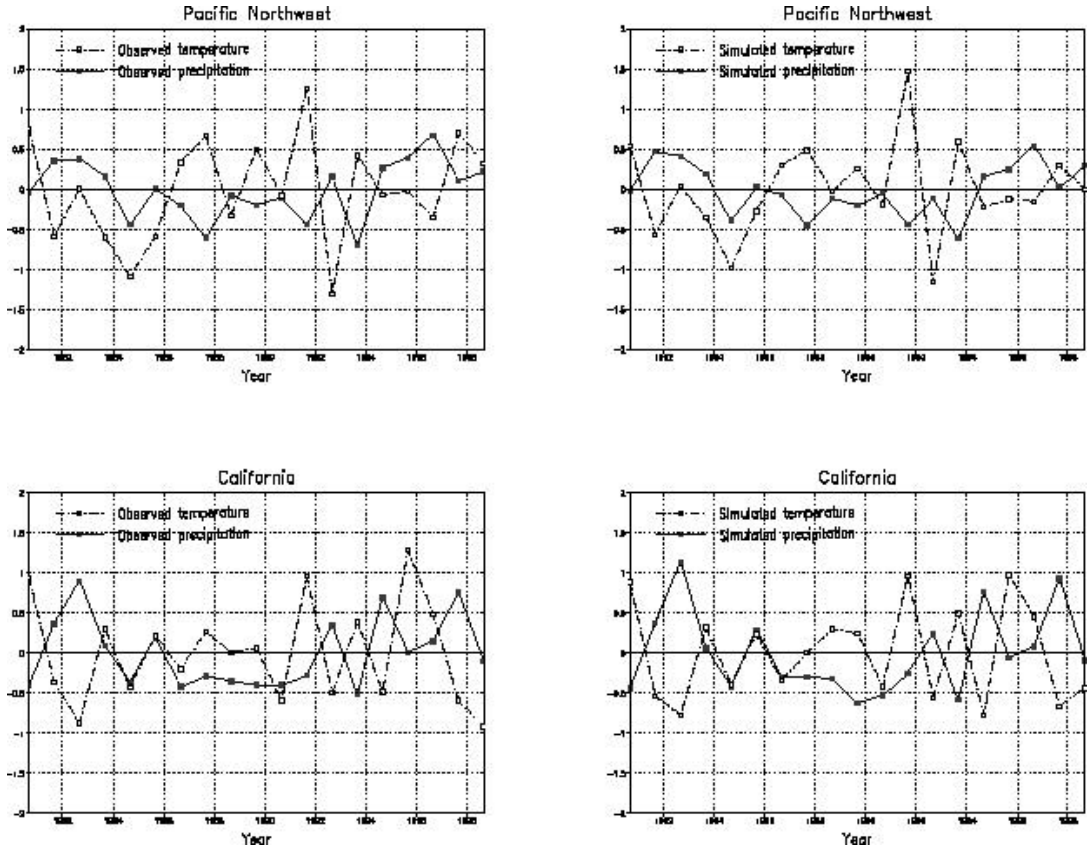
Pacific Northwest
Observed temperature
Observed precipitation
Year
Pacific Northwest
Simulated temperature
Simulated precipitation
Year
California
Observed temperature
Observed precipitation
Year
California
Simulated temperature
Simulated precipitation
Year

Figure 3

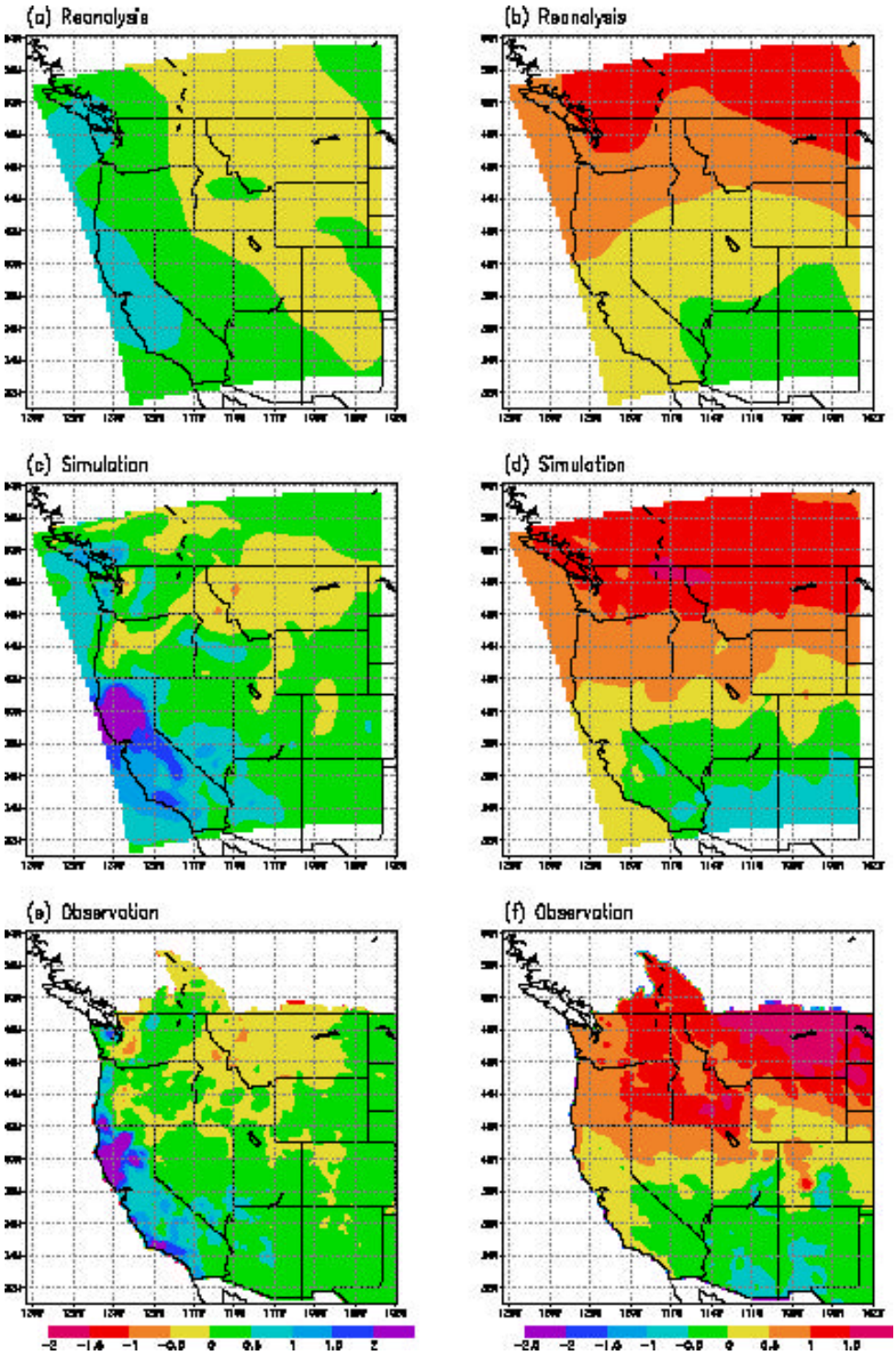
(a) Reanalysis
(b) Reanalysis
(c) Simulation
(d) Simulation
(e) Observation
(f) Observation

Figure 4

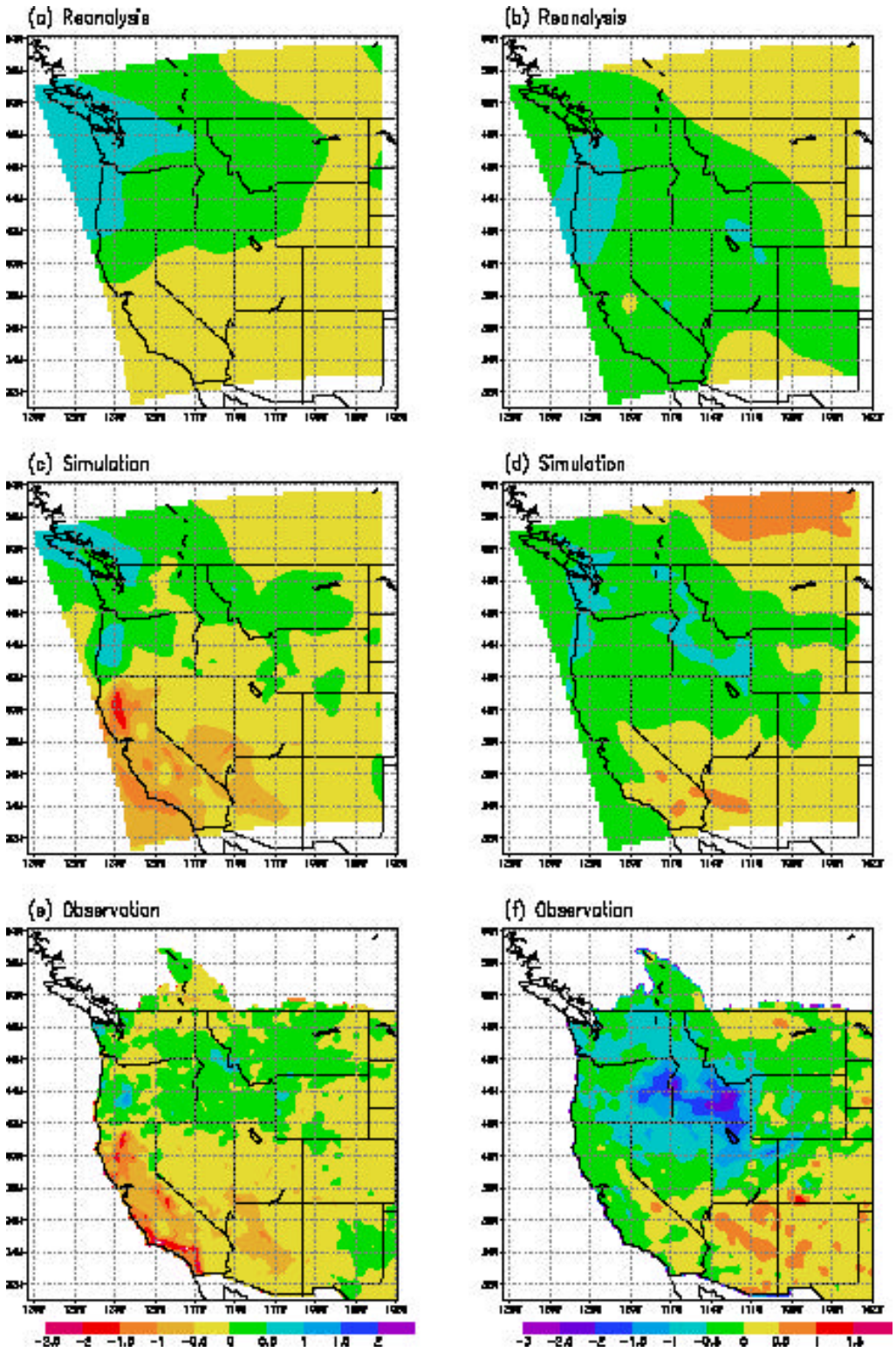
(a) Reanalysis
(b) Reanalysis
(c) Simulation
(d) Simulation
(e) Observation
(f) Observation

Figure 5

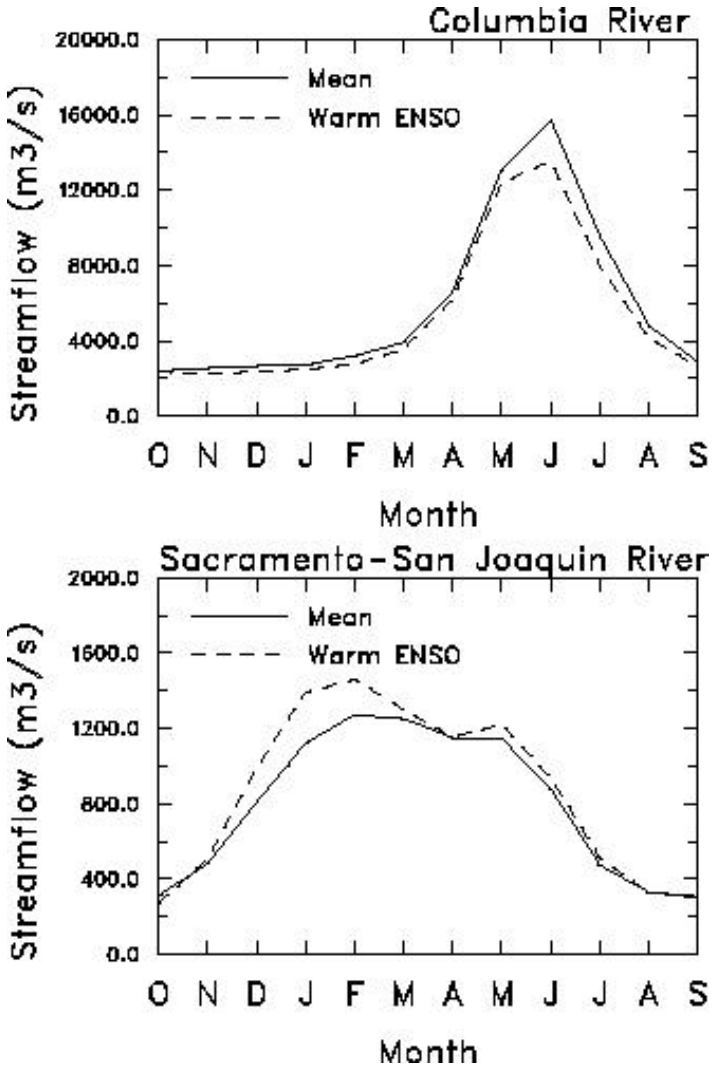
Columbia River
Mean
Warm ENSO
Streamflow (m3/s)
20000.0
16000.0
12000.0
8000.0
4000.0
0.0
O N D J F M A M J J A S
Month
Sacramento-San Joaquin River
Mean
Warm ENSO
Streamflow (m3/s)
2000.0
1600.0
1200.0
800.0
400.0
0.0
O N D J F M A M J J A S
Month

Figure 6

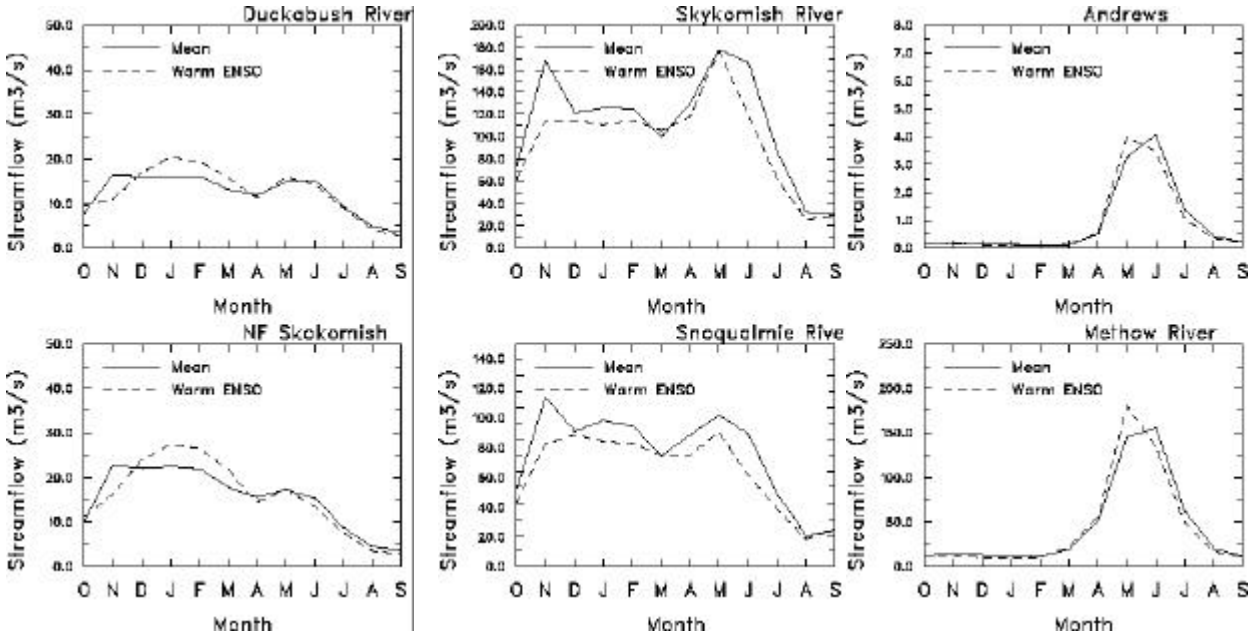
Duckabush River
Skykomish River
Andrews
NF Skokomish
Snoqualmie Rive
Methow River
Mean
Warm ENSO
Streamflow (m3/s)
Month
O N D J F M A M J J A S

Figure 7

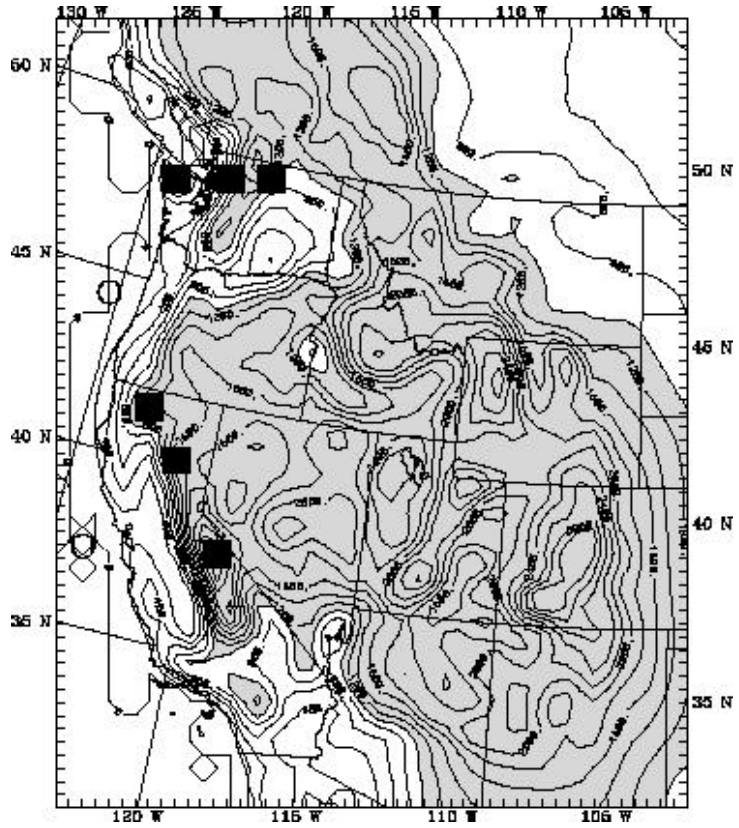
130 W
125 W
120 W
115 W
110 W
105 W
60 N
55 N
50 N
45 N
40 N
35 N
120 W
115 W
110 W
105 W

Figure 8

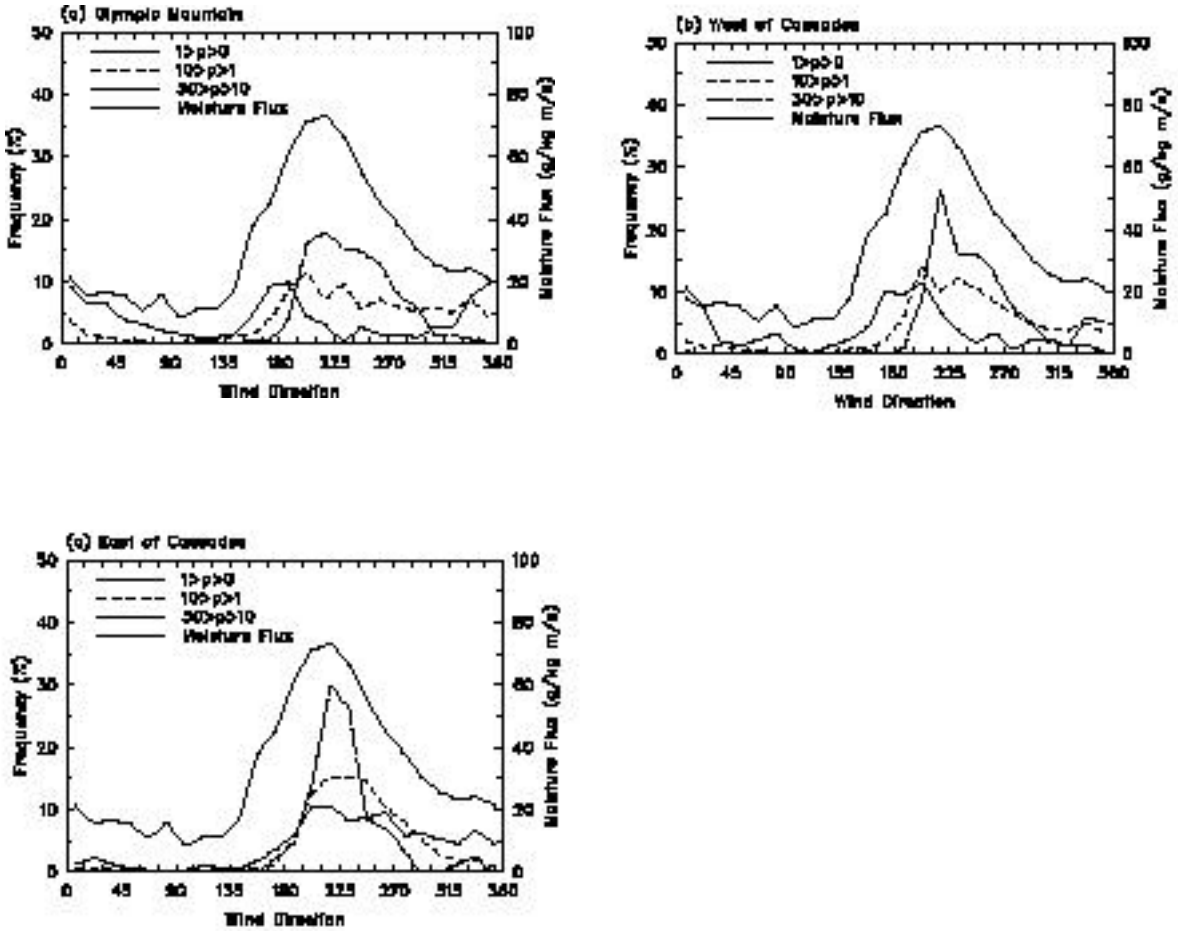
(a) Olympic Mountains
(b) West of Cascades
(c) East of Cascades
Frequency (%)
Moisture Flux (g/kg m/s)
Wind Direction
Moisture Flux

Figure 9

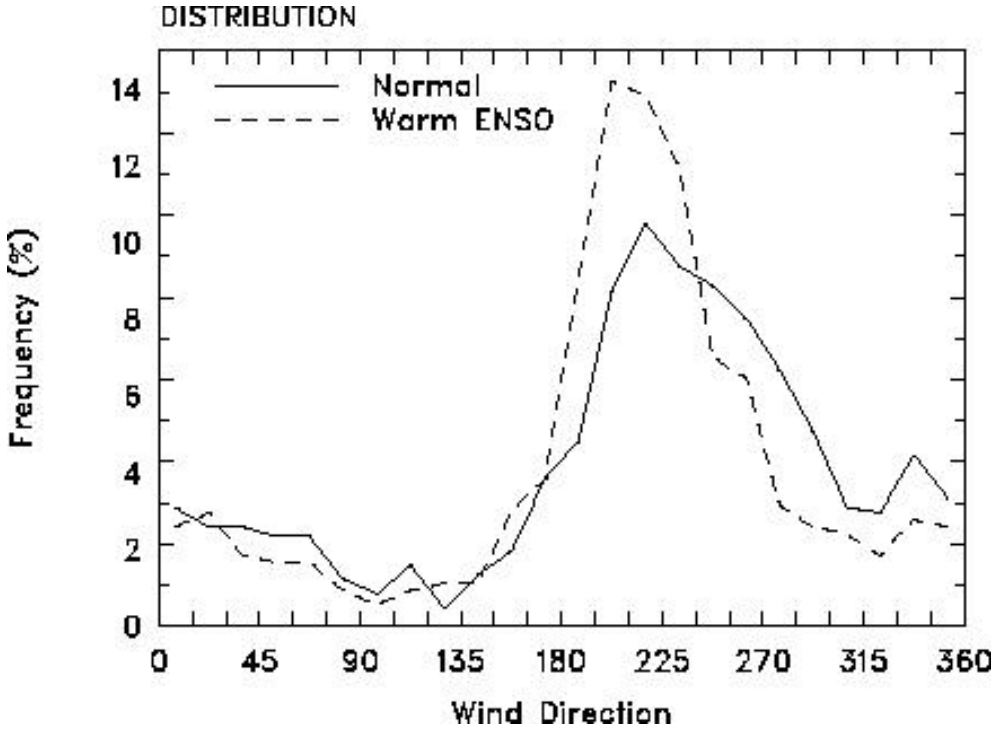
DISTRIBUTION
Normal
Warm ENSO
Frequency (%)
0
2
4
6
8
10
12
14
0
45
90
135
180
225
270
315
360
Wind Direction

Figure 10

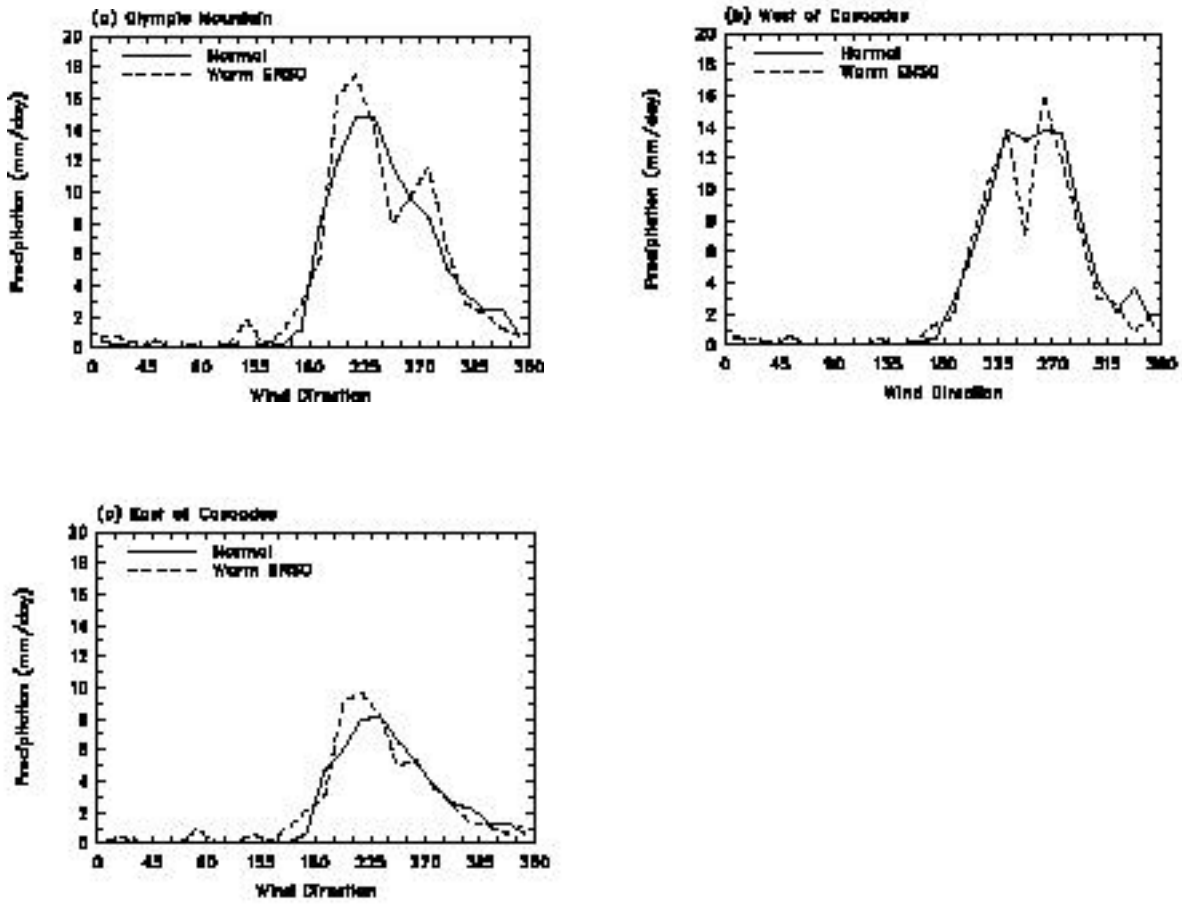
(a) Olympic Mountain
Normal
Precipitation (mm/day)
Wind Direction
(b) West of Cascades
Normal
Precipitation (mm/day)
Wind Direction
(c) East of Cascades
Normal
Precipitation (mm/day)
Wind Direction

Figure 11

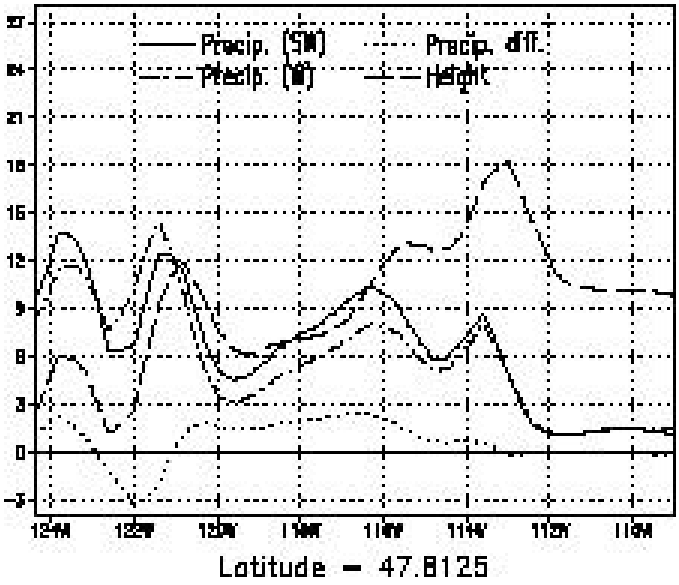

Figure 12

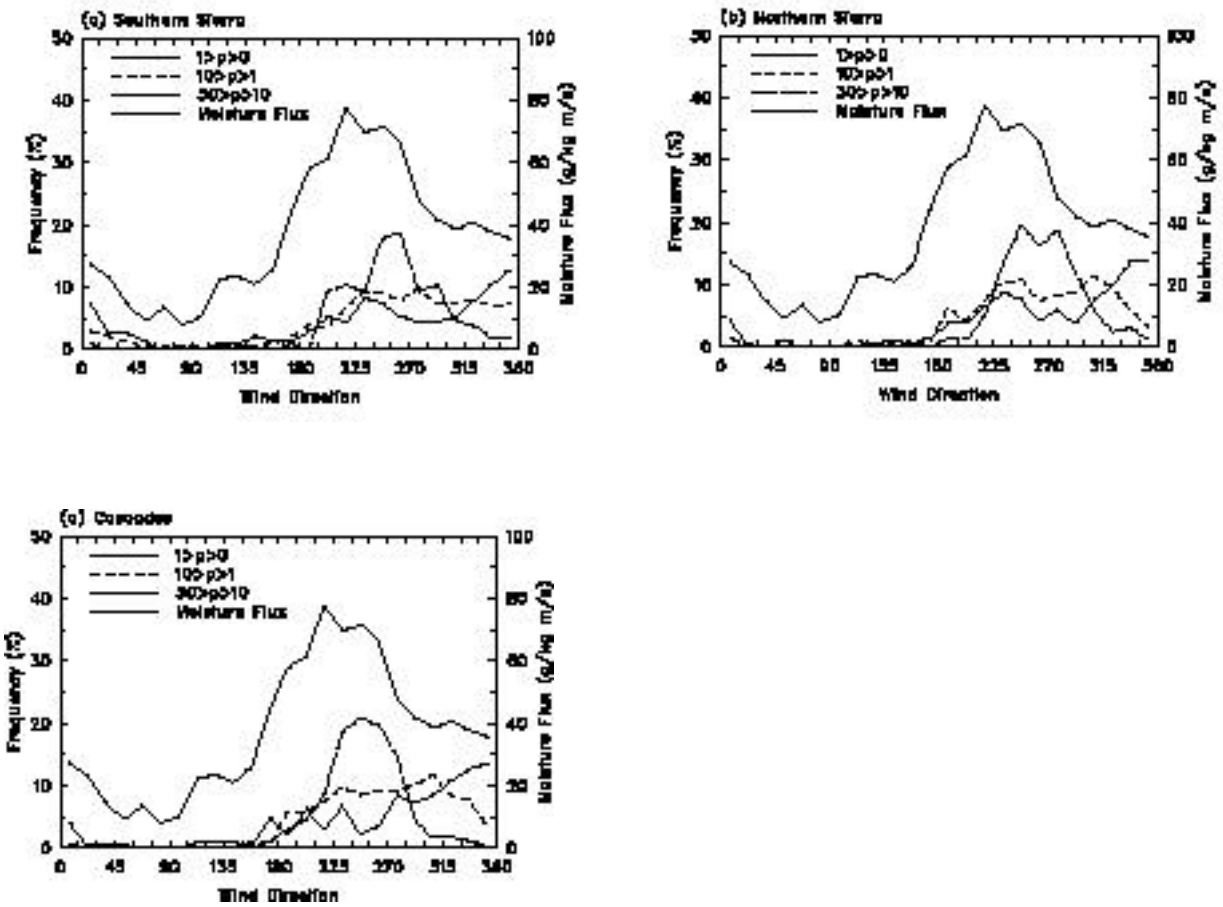
(a) Southern Sierra
(b) Northern Sierra
(c) Cascades
Frequency (%)
Moisture Flux (g/kg m/s)
Wind Direction
Moisture Flux

Figure 13

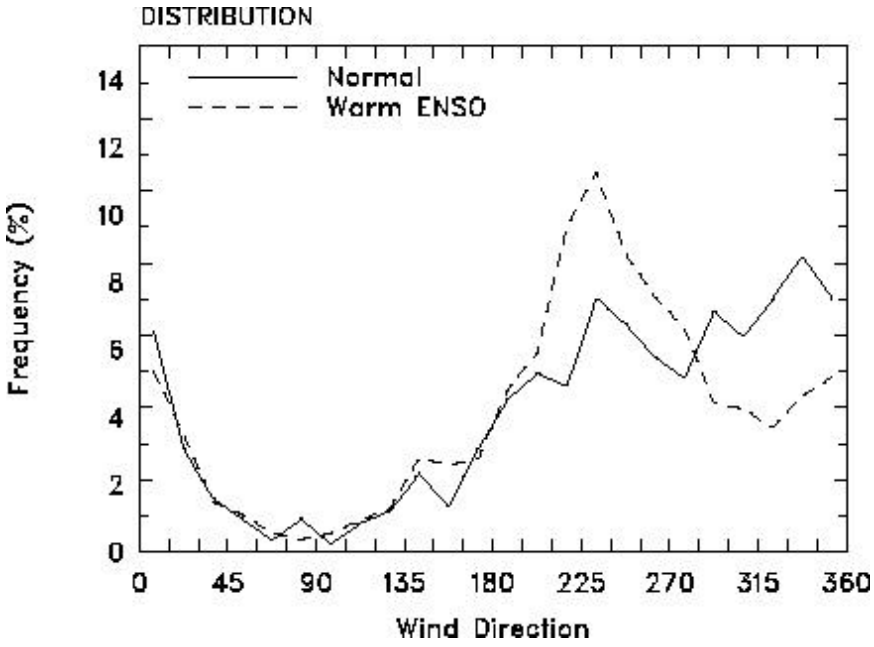
DISTRIBUTION
Normal
Warm ENSO
Frequency (%)
0
2
4
6
8
10
12
14
0
45
90
135
180
225
270
315
360
Wind Direction

Figure 14

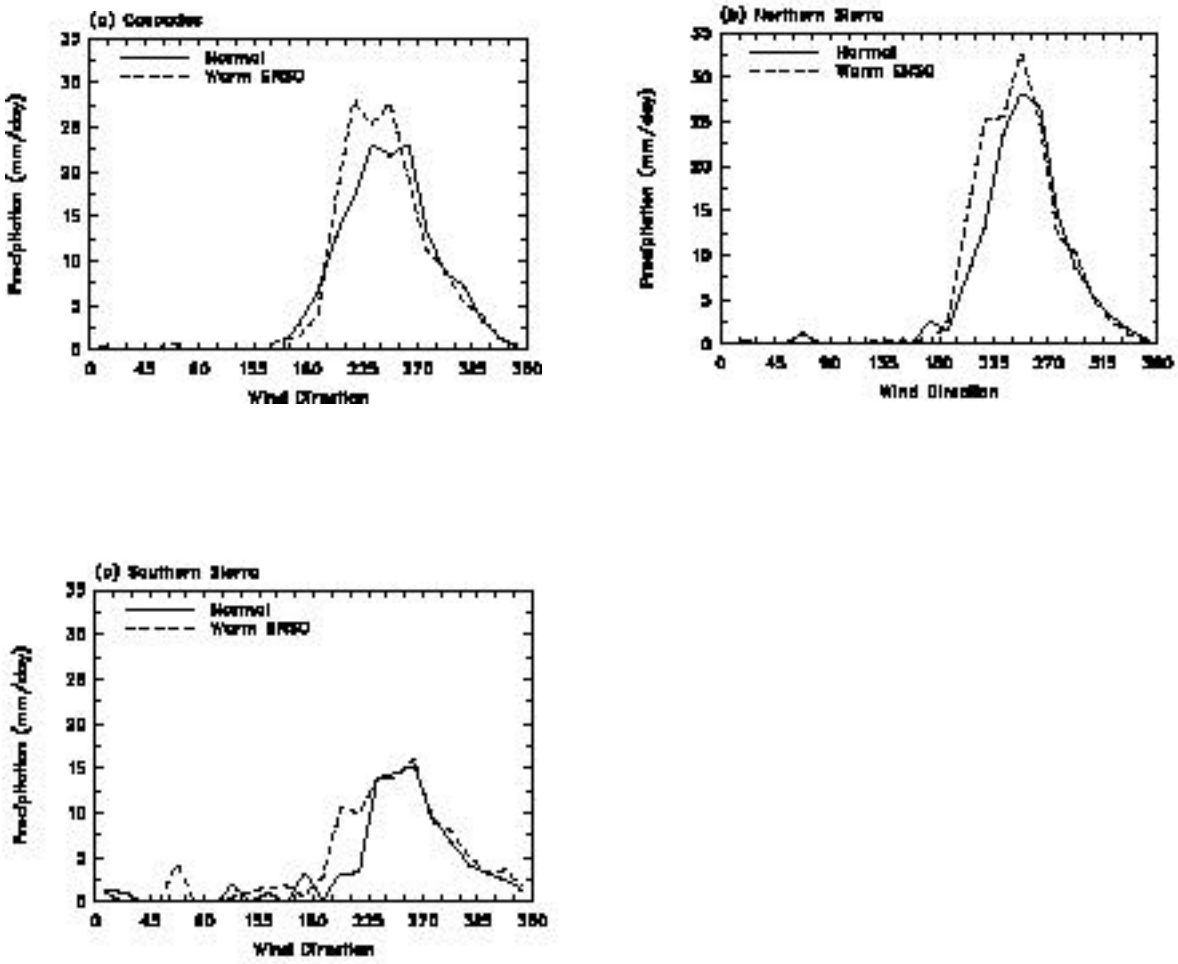
(a) Cascades
Normal
Warm
Precipitation (mm/day)
Wind Direction
(b) Northern Sierra
Normal
Warm
Precipitation (mm/day)
Wind Direction
(c) Southern Sierra
Normal
Warm
Precipitation (mm/day)
Wind Direction

Figure 15